ACS APPLIED MATERIALS & INTERFACES

Letter

www.acsami.org

Template-Free Synthesis of Hematite Photoanodes with Nanostructured ATO Conductive Underlayer for PEC Water Splitting

Degao Wang,[†] Yuying Zhang,[†] Jianqiang Wang,[†] Cheng Peng,*[,†] Qing Huang,[†] Shao Su,[‡] Lianhui Wang,*[,‡] Wei Huang,[‡] and Chunhai Fan[†]

[†]Division of Physical Biology, and Bioimaging Center, Shanghai Synchrotron Radiation Facility, Key Laboratory of Interfacial Physics and Technology, Shanghai Institute of Applied Physics Chinese Academy of Sciences, Shanghai 201800, China

[‡]Key Laboratory for Organic Electronics and Information Displays and Institute of Advanced Materials, Nanjing University of Posts and Telecommunications, Nanjing 210023, China

Supporting Information

ABSTRACT: Hematite is a promising semiconductor candidate for PEC water splitting. However, hematite is far well short of the theoretical value of solar-to-fuel conversion efficiency because of the fast recombination of photogenerated carriers. To address this limitation, a facile template-free preparation of hematite photoanode with nanostructured ATO (antimony-doped tin oxide) conductive underlayer served as a scaffold to transport photogenerated electron was developed to decrease the recombination opportunities of the carriers. Furthermore, the constructed ATO scaffold could also increase the light absorption of hematite and the number of the carriers, resulting in better PEC performance of hematite.

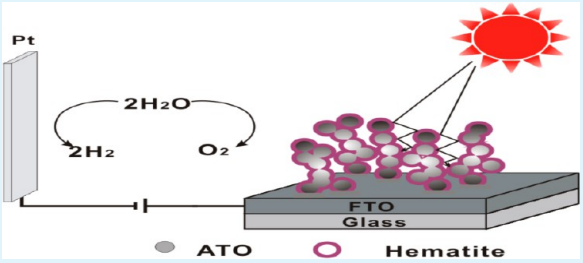

KEYWORDS: *photoelectrochemical, water splitting, nanostructured hematite photoanode, antimony-doped tin oxide, conductive underlayer*

INTRODUCTION

Photoelectrochemical (PEC) water splitting, a direct channel towards converting solar energy to hydrogen, has attracted worldwide interest since the first demonstration in 1972 by Honda and Fujishima.[1] As a promising photoanode material in PEC water splitting, hematite has been widely investigated due to its favorable optical band gap (2.1 eV) for sufficiently broad visible light absorption and excellent stability under the operation conditions.[2−5] However, hematite also suffers from two conflicting properties of poor visible light adsorption derived from indirect band transition and worse carrier separation due to rapid recombination.[6−8] These disadvantages severely limit the PEC efficiency of hematite.

To address these limitations, one approach is dimension and morphology control of hematite nanostructures, for example one-dimensional (1D) of nanorods and nanotubes,[9−14] two-dimensional (2D) of nanoplates and nanofilms, and three-dimensional (3D) dendritic or porousnanostructures.[15] These unique nanostructures are often designed and fabricated less than 50 nm to circumvent poor carrier transport by minimizing the distance of minority diffusion. Another approach is doping element into hematite surface for improving charge transport ability or surface modification on hematite for surface state passivation to reduce surface recombination.[16−21] Recently, fluorine-doped tin oxide (FTO) substrate modification also benefits the PEC performance enhancement of hematite. For instance, modification of SiO_x and Ga_2O_3 ultrathin films on FTO substrate improves the crystallinity and uniformity of ultrathin hematite films.[22,23] While modification of Nb_2O_5 and TiO_2 ultrathin films on FTO substrate improves the PEC efficiency of hematite ultrathin films by suppressing electron back injection resulting in carrier recombination near the interface between hematite and FTO substrate.[24] Very recently, Peng et al. directly built the nanostructured antimony-doped tin oxide (nano-ATO) conductive underlayer via commercial ATO nanoparticles for improving the PEC performance of TiO_2 ultrathin films.[25] Furthermore, Moir et al. fabricated nano-ATO conductive underlayer via polystyrene nanospheres as the template.[26] The introduced nano-ATO conductive underlayers enhanced the water splitting performance via reducing electron-charge recombination and increasing light adsorption. Inspired by their work, we developed a facile template-free method of preparing hematite photoanode for PEC water splitting enhancement. In this communication, the commercial ATO nanoparticles with the average size of 13−22 nm were utilized to build the nano-ATO conductive underlayer and atmosphere pressure chemical vapor deposition (APCVD) was employed to load hematite. Considering the readily available commercial ATO nanoparticles and the convenient APCVD process, the

Received: November 17, 2013
Accepted: December 16, 2013
Published: December 16, 2013

facile template-free method is more suitable to prepare large-scale hematite photoanode for efficient PEC water splitting.

EXPERIMENTAL SECTION

Fluorine-doped tin oxide coated glass substrate (FTO, TEC15, NSG) were precleaned with acetone, ethanol and water. Then 0.05g antimony-doped tin oxide nanoparticles (Alfa Aesar, ratio of Sb_2O_5/SnO_2 is 15:85) of average size of 13−22 nm was dissolved into 4 mL of ethanol to prepare the colloidal solution and 50 μL of ATO colloids were dropped on FTO (3×3 cm^2) to prepare the porous nano-ATO films. These nano-ATO films were then annealed in air at 500 °C for 1 h in a box oven and then 0.2 g of ferric actylacetonate was employed to load hematite via APCVD. Both of the bare FTO and nano-ATO substrate were put on the crucible at 500 °C for 90 min and then at 800 °C for 10 min further annealing treatment. Therefore, hematite nanostructured photoanodes with nano-ATO underlayer were fabricated by soldering copper wire on the bare potion of FTO. All samples were sealed on all edges with epoxy resin except a bare area of 0.4 cm^2 for photo excitation.

The morphologies of all samples were characterized by scanning electron microscope (SEM, JME2011, JEOL, Japan). Electrochemical impedance spectra (EIS) were collected by Autolab electrochemical workstation (Metrohm AG, Switzerland).

The electrochemical AC impedance spectroscopy were performed both in the dark configuration system in 1.0 M NaOH solution with a sinusoidal perturbation with 50 mV amplitude and frequencies ranging from 100 kHz to 0.1 Hz. Capacitance values were derived from the impedance-potential The hematite photoanode with a bare portion of FTO substrate was fabricated by soldering with copper wire and all samples were sealed on all edges with epoxy resin except a bare area of 0.4 cm^2 for photo excitation. All photoelectrochemical measurements were tested in a three electrode configuration with the Pt counter electrode, the Ag/AgCl reference electrode and the working electrode of the as-prepared photoanodes. An aqueous solution of 1.0 M NaOH (pH 13.6) after deaerating with a nitrogen flow was filled in a quartz PEC cell as the electrolyte. A solar simulator (Newport, model SP 94023A) coupled to a filter (AM 1.5G) using 150 W Xenon lamp was used as the light source. The light power density of 1000 W/m^2 was measured with a power meter (Newport, 91150 V). In a typical experiment, the photoanode with 0.4 cm^2 area of photoresponse surface was immersed in the electrolyte in PEC cell and illuminated under the artificial simulated sunlight initiated from the infrared xenon lamp. Incident photon-to-current conversion efficiency (IPCE) spectra were measured by an electrochemical station with a solar simulator, coupled to an infrared filter. We used different wavelength filter equipped to the solar simulator to get the different light distribution to measure the IPCEs of hematite electrodes in the dark condition and Mott−Schottky plots were generated from the capacitance values. The collected potentials vs. Ag/AgCl were converted to the reversible hydrogen electrode (RHE) scale according to the Nernst equation

$$E_{RHE} = E_{Ag/AgCl} + 0.059pH + E^0_{Ag/AgCl} \quad (1)$$

where E_{RHE} was the converted potential vs. RHE, $E^0_{Ag/AgCl}$ was 0.1976 V at 25 °C, and $E_{Ag/AgCl}$ was the experimental potential against the Ag/AgCl reference. Because the solution pH value was 13.6, the $E_{Ag/AgCl}$ could be converted to E_{RHE} according to the following equation

$$E_{RHE} = E_{Ag/AgCl} + 1 \quad (2)$$

The carrier densities were calculated from the slope of Mott−Schottky plot by the following equation

$$(1/C)^2 = (2/e_0\varepsilon\varepsilon_0 N_d)(E - E_{FB} - kT/e_0) \quad (3)$$

where C was capacitance (F/cm^2), e_0 was the electron charge, ε was the hematite dielectric constant of 80, ε_0 was the permittivity of vacuum, N_d was the carrier density, E was the electrode applied potential, E_{FB} was the flat band potential, k was the Boltzmann's constant, and T was the temperature.

RESULTS AND DISSCUSION

In our experiments, we dispersed commercial ATO nanoparticles into deionized water to form nano-ATO conductive underlayer on FTO substrate via spin-coating. Then ferric actylacetonate was utilized as the hematite precursor for loading hematite nanostructures on the as-prepared nano-ATO conductive underlayer via APCVD. In the following, the hematite photoanode with nano-ATO conductive underlayer was named as FTO-nano ATO/hematite photoanode and the one without nano-ATO conductive underlayer was named as FTO/hematite photoanode, respectively. As shown in Figure 1,

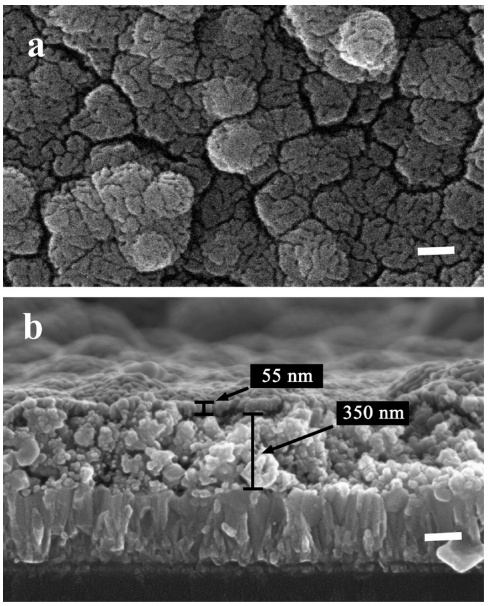

Figure 1. SEM images of (a) cross-sectional image and (b) FTO-nanoATO/hematite photoanode, the white bar represents 100 nm.

the hematite nanostructured thin film was formed on nano-ATO conductive underlayer, similar morphology with the hematite nanostructured film formed on the bare FTO substrate (see Figure 2a). Furthermore, the thickness of hematite film was ~50 nm and the thickness of nano-ATO conductive underlayer was ~350 nm. Of note, after loading hematite, the size of nanoparticles of the nano-ATO conductive underlayer was obviously larger than that of the pristine ATO nanoparticles (less than 50 nm in Figure 2b), which indicated that the hematite precursor was diffused into nano-ATO conductive underlayer and the hematite was successfully loaded into nano-ATO conductive underlayer via APCVD. Therefore,

dx.doi.org/10.1021/am405137p | ACS Appl. Mater. Interfaces 2014, 6, 36−40

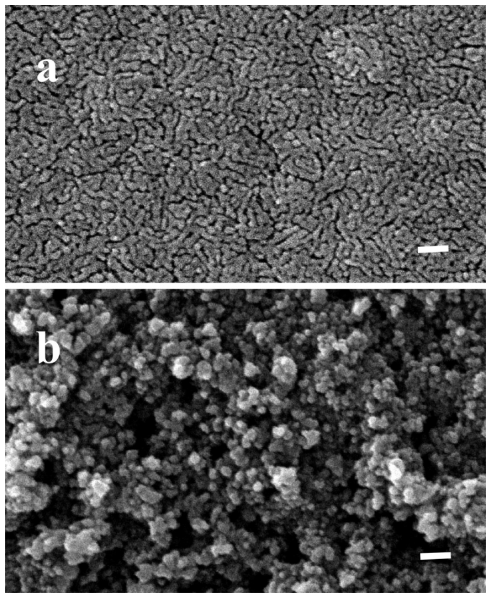

Figure 2. SEM images of (a) FTO/hematite photoanode and (b) nano-ATO conductive underlayer, the scale bar represents 100 nm in each image.

nano-ATO conductive underlayer loaded more hematite nanoparticles in FTO-nano ATO/hematite photoanode, compared with the FTO/hematite photoanode.

The PEC performance was investigated by a three-electrode system under the voltage scan speed of 0.01 V/s in the range from 0.60 V to 1.80 V vs. RHE (reversible hydrogen electrode) in a quartz PEC cell fulfilled with the aqueous solution of 1.0 M NaOH (pH 13.6) after deaerating with N_2 for 30 min, and the photocurrent density-applied potential ($J-V$) scan was measured with the AM 1.5G simulated solar light at 100 mW/cm^2 on 0.4 cm^2 photoresponse area of photoanode. As shown in Figure 3a, the photocurrent density of FTO-nanoATO/hematite photoanode reached 0.83 mA/cm^2 at 1.23 V vs. RHE, 3 times higher than 0.26 mA/cm^2 of FTO/hematite photoanode. As control, a negligible photocurrent density was observed from the bare ATO photoanode (see Figure 4), which was well consistent with the characteristics of no visible light absorption due to the large optical bandgap of ATO. Correspondingly, the incident-photo-to-current-efficiencies (IPCE) of both photoanodes were presented in Figure 3b. The IPCE value of FTO-nanoATO/hematite photoanode achieved 8.3% at 380 nm with the bias voltage of 1.3 V vs. RHE, 3 times higher than FTO/hematite photoanode. Furthermore, the onset potential of both FTO-nanoATO/hematite photoanode and FTO/hematite photoanode were ~0.7 V, indicating the nano-ATO conductive underlayer had no influence on the onset potential of hematite nanostructured film. Therefore, introducing nano-ATO conductive underlayer between hematite nanostructured film and FTO substrate largely enhanced the photoelectrochemical water splitting performance.

UV−vis absorption spectra were then employed to investigate the optical properties of both as-prepared photoanodes. As shown in Figure 5, the FTO-nanoATO/hematite photoanode exhibited better visible light absorption capacity compared with the FTO/hematite photoanode in range from 350 to 700 nm, which indicated that introducing nano-ATO conductive underlayer largely increased the solar light

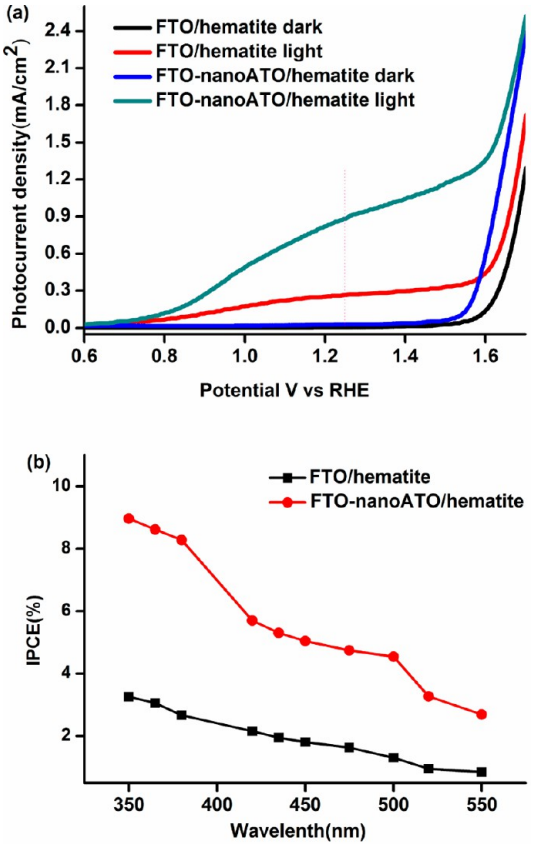

Figure 3. (a) $J-V$ curves and (b) IPCE spectra of FTO-nanoATO/hematite photoanode and FTO/hematite photoanode.

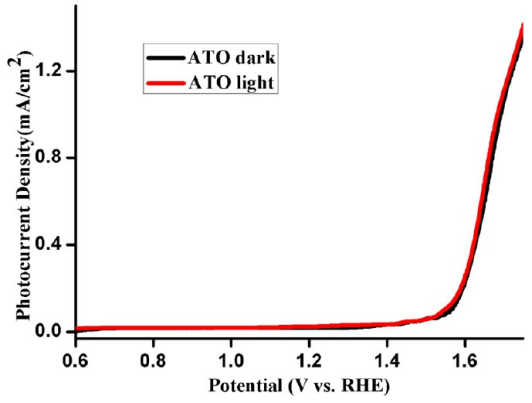

Figure 4. The $J-V$ curves of nano-ATO conductive underlayer in the light and in the dark conditions.

adsorption of hematite. Considering nano-ATO conductive underlayer performs no adsorption in range of visible lights, the nano-ATO conductive underlayer helps to enhance solar light adsorption in two ways, loading more amount of hematite and protracting the optical path length. Due to the disordered nanostructures in nano-ATO conductive underlayer, the optical path length was increased and the trapping of light was increased correspondingly. Both of the beneficial factors largely increased the solar light adsorption of hematite-ATO photoanode and therefore contributed to the enhancement of PEC performance.

Electrochemical impedance spectroscopy (EIS) was then employed to determine the capacities and resistances within the

dx.doi.org/10.1021/am405137p | ACS Appl. Mater. Interfaces 2014, 6, 36−40

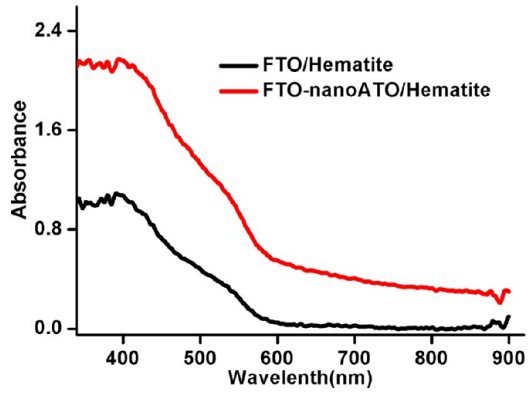

Figure 5. UV−vis spectra of FTO-nanoATO/hematite photoanode and FTO/hematite photoanode.

PEC cell in the dark condition. The as-prepared photoanodes were both investigated at 0.8 and 1.6 V vs. RHE, corresponding to non-Faradaic region and Faradaic region, respectively. The obtained Nyquist plots (see Figure 6) were molded via Randle's

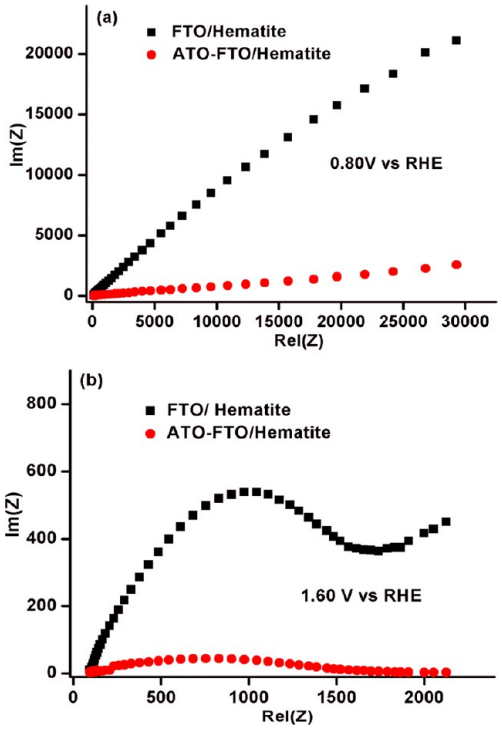

Figure 6. Nyquist plots of FTO/hematite and ATO-FTO/hematite photoanode at (a) 0.80 V vs. RHE and (b) 1.60 V vs. RHE.

equivalent and the resultant capacitances and resistances were shown in Table 1. In detail, the series resistance of hematite-ATO photoanode was 33.81 Ω at 0.8 V vs. RHE, only one-third of the pristine hematite photoanode. Furthermore, the charge transport resistance of FTO-nanoATO/hematite photoanode was 146.9 Ω, almost 20 times smaller than that of FTO/hematite photoanode. It suggested that introducing nano-ATO conductive underlayer reduced electron-charge recombination via effective electron collection by considering that small charge transport resistance facilitated electron conductivity. Conversely, the capacitance of FTO-nanoATO/hematite photoanode was 74.0 μF, ~4.5 times larger than that of FTO/hematite photoanode. It demonstrated that introducing nano-

Table 1. EIS Data of FTO-nanoATO/hematite Photoanode and FTO/Hematite Photoanode

V_{app} vs. RHE		FTO/hematite	FTO-nanoATO/hematite
0.8 V	R_{ct} (Ω)	2673	146.9
	C_N (μF)	16.1	74
	R_s (Ω)	112.1	33.81
1.6 V	R_{ct} (Ω)	779.3	65.72
	C_N (μF)	9.2	55.4
	R_s (Ω)	103.1	37.46

ATO conductive underlayer reduced electron-charge recombination via effective charge accumulation on surface by considering that large capacitance represents large surface charge density. The similar resultant trends of capacitance and resistances were observed under the potential of 1.6 V vs. RHE too. Moreover, the Mott-Schottky plots were also obtained from EIS measurements in the dark condition. According to the Mott−Schottky plots in Figure 7, the calculated electron

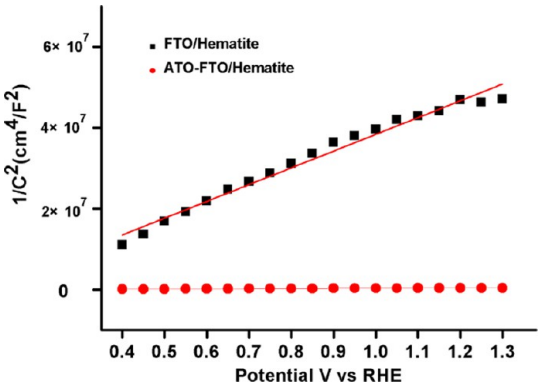

Figure 7. Mott−Schottky plots of FTO-nanoATO/hematite photoanode and FTO/hematite photoanode.

density of FTO-nanoATO/hematite photoanode was 4.1×10^{22} cm^{-3}, 2 orders of magnitude higher than that of FTO/hematite anode (4.3×10^{20} cm^{-3}). The introduced nano-ATO conductive underlayer might play as an effective carrier transport layer for reducing electron-hole recombination and increasing carrier number. Therefore, the EIS results demonstrate convincingly that introducing nano-ATO conductive underlayer favors PEC water splitting via effectively reducing electron-charge recombination.

CONCLUSION

We developed a facile template-free method for preparing hematite photoanode with nano-ATO conductive underlayer for improving PEC water splitting performance. Importantly, introducing the nano-ATO conductive underlayer between hematite and FTO substrate enhanced the photocurrent density to 0.83 mA/cm^2, 3-fold higher than the pristine photoanode without nano-ATO conductive underlayer. Investigated by UV-vis adsorption spectra and EIS measurements, it is found that introducing as-prepared nano-ATO conductive underlayer largely increased light absorption and effectively reducing electron-charge recombination, which benefits the PEC performance of hematite. Furthermore, because of the readily available commercial raw material and the convenient APCVD process, this facile method is suitable for preparing large scale and putting PEC into practice.

dx.doi.org/10.1021/am405137p | ACS Appl. Mater. Interfaces 2014, 6, 36−40

■ ASSOCIATED CONTENT

Supporting Information

The UV−vis spectrum of ATO scaffold on FTO substrate. This material is available free of charge via the Internet at http://pubs.acs.org.

■ AUTHOR INFORMATION

Corresponding Authors

*E-mail: pengcheng@sinap.ac.cn.
*E-mail: iamlhwang@njupt.edu.cn.

Notes

The authors declare no competing financial interest.

■ ACKNOWLEDGMENTS

The authors acknowledge the financial support by the by the National Natural Science Foundation 51102272 and 91127001, and Foundation of State Key Laboratory of Coal Combustion FSKLCC1209.

■ REFERENCES

(1) Fujishima, A.; Honda, K. *Nature* **1972**, *238*, 37−38.
(2) Grätzel, M. *Nature* **2001**, *414*, 338−344.
(3) Li, Y.; Zhang, J. Z. *Laser Photonics Rev.* **2010**, *4*, 517−528.
(4) Katz, M. J.; Riha, S. C.; Jeong, N. C.; Martinson, A. B. F.; Farha, O. K.; Hupp, J. T. *Coord. Chem. Rev.* **2012**, *256*, 2521−2529.
(5) Lin, Y.; Zhou, S.; Sheehan, S. W.; Wang, D. *J. Am. Chem. Soc.* **2011**, *133*, 2398−2401.
(6) Zhong, D. K.; Sun, J.; Inumaru, H.; Gamelin, D. R. *J. Am. Chem. Soc.* **2009**, *131*, 6086−6087.
(7) Sivula, K.; Zboril, R.; Le Formal, F.; Robert, R.; Weidenkaff, A.; Tucek, J.; Frydrych, J.; Grätzel, M. *J. Am. Chem. Soc.* **2010**, *132*, 7436−7444.
(8) Wang, H.; Turner, J. A. *J. Electrochem. Soc.* **2010**, *157*, F173−F178.
(9) Vayssieres, L.; Beermann, N.; Lindquist, S.-E.; Hagfeldt, A. *Chem. Mater.* **2000**, *13*, 233−235.
(10) Qin, D.-D.; Tao, C.-L.; In, S.-i.; Yang, Z.-Y.; Mallouk, T. E.; Bao, N.; Grimes, C. A. *Energy Fuels* **2011**, *25*, 5257−5263.
(11) Mohapatra, S. K.; John, S. E.; Banerjee, S.; Misra, M. *Chem. Mater.* **2009**, *21*, 3048−3055.
(12) Li, L.; Yu, Y.; Meng, F.; Tan, Y.; Hamers, R. J.; Jin, S. *Nano Lett.* **2012**, *12*, 724−731.
(13) Yin, Z. Y.; Wang, Z.; Du, Y. P.; Qi, X. Y.; Huang, Y. Z.; Xue, C.; Zhang, H. *Adv. Mater.* **2012**, *24*, 5374−5378.
(14) Wang, P.; Wang, D.; Lin, J.; Li, X.; Peng, C.; Gao, X.; Huang, Q.; Wang, J.; Xu, H.; Fan, C. *ACS Appl. Mater. Interfaces* **2012**, *4*, 2295−2302.
(15) Tilley, S. D.; Cornuz, M.; Sivula, K.; Grätzel, M. *Angew. Chem. Int. Ed.* **2010**, *49*, 6405−6408.
(16) Klahr, B.; Gimenez, S.; Fabregat-Santiago, F.; Hamann, T.; Bisquert, J. *J. Am. Chem. Soc.* **2012**, *134*, 4294−4302.
(17) Le Formal, F.; Tetreault, N.; Cornuz, M.; Moehl, T.; Gratzel, M.; Sivula, K. *Chem. Sci.* **2011**, *2*, 737−743.
(18) Hu, Y.-S.; Kleiman-Shwarsctein, A.; Forman, A. J.; Hazen, D.; Park, J.-N.; McFarland, E. W. *Chem. Mater.* **2008**, *20*, 3803−3805.
(19) Shen, S.; Jiang, J.; Guo, P.; Kronawitter, C. X.; Mao, S. S.; Guo, L. *Nano Energy* **2012**, *1*, 732−741.
(20) Hahn, N. T.; Mullins, C. B. *Chem. Mater.* **2010**, *22*, 6474−6482.
(21) Cheng, W.; He, J.; Sun, Z.; Peng, Y.; Yao, T.; Liu, Q.; Jiang, Y.; Hu, F.; Xie, Z.; He, B.; Wei, S. *J. Phys. Chem. C* **2012**, *116*, 24060−24067.
(22) Le Formal, F.; Grätzel, M.; Sivula, K. *Adv. Funct. Mater.* **2010**, *20*, 1099−1107.
(23) Hisatomi, T.; Brillet, J.; Cornuz, M.; Le Formal, F.; Tetreault, N.; Sivula, K.; Gratzel, M. *Faraday Discuss.* **2012**, *155*, 223−232.
(24) Hisatomi, T.; Dotan, H.; Stefik, M.; Sivula, K.; Rothschild, A.; Grätzel, M.; Mathews, N. *Adv. Mater.* **2012**, *24*, 2699−2702.
(25) Peng, Q.; Kalanyan, B.; Hoertz, P. G.; Miller, A.; Kim, D. H.; Hanson, K.; Alibabaei, L.; Liu, J.; Meyer, T. J.; Parsons, G. N.; Glass, J. T. *Nano Lett.* **2013**, *13*, 1481−1488.
(26) Moir, J.; Soheilnia, N.; O'Brien, P.; Jelle, A.; Grozea, C. M.; Faulkner, D.; Helander, M. G.; Ozin, G. A. *ACS Nano* **2013**, *7*, 4261−4274.